https://doi.org/10.33271/nvngu/2026-4/089

M. A. Kovalenko[1],
orcid.org/0000-0002-5602-2001,
V. V. Chumack[1],
orcid.org/0000-0001-8401-7931,
D. V. Tsyplenkov[*2,3],
orcid.org/0000-0002-0378-5400,
R. P. Dukhno[1],
orcid.org/0009-0008-9506-2234,
D. D. Horbatko[1],
orcid.org/0009-0007-6376-2829

1 – National Technical University of Ukraine "Igor Sikorsky Kyiv Polytechnic Institute", Kyiv, Ukraine
2 –Dnipro University of Technology, Dnipro, Ukraine
3 – Dnipropetrovsk Scientific Research Institute of Forensic Expertise, Dnipro, Ukraine
* Corresponding author e-mail: tsyplenkov.d.v@nmu.one

COMPARISON OF IMPULSE PROCESSES IN SPATIALLY SHIFTED RING-LIKE CORES MADE OF FERRITE AND THIN SHEET STEEL

Purpose. Development of a numerical simulation model of pulse processes of magnetic cores made of ferrite and thin-sheet electrical steel in order to estimate the magnitude of pulse overvoltages.

Methodology. The distribution of the electromagnetic field and eddy currents was calculated using the finite element method. Computer-aided design tools were used to develop geometric models of the computational domain of the studied processes in ring-shaped cores. The theory of transient processes and the laws of electric circuits were used to excite pulse processes in the studied system.

Findings. A three-dimensional numerical ring-field mathematical model of pulse excitation of ring-shaped cores made of different materials of electrical steel of the sensor and inductor was developed, which is used to diagnose interturn short circuits of the filled windings. The model allows determining the time dependences of current, voltage and the nature of the change in magnetic flux during the passage of the pulse excitation front. The distributions of the electromagnetic field, eddy currents and the dynamics of their attenuation were obtained for different values of the magnetic permeability and electrical conductivity of the materials. The obtained results allow us to quantitatively assess the influence of material parameters on pulse processes, to determine the limits of efficiency of using ferrite and cores from different types of electrical steel in high-frequency diagnostic systems, sensors and energy converters.

Originality. The results of the analysis of numerical simulation modeling of the studied system showed that, depending on the type of core material, wave penetration processes with minimal losses are inherent in ferrite material. In thin-sheet steel, eddy currents in each individual sheet have a significant effect on pulse shielding, which significantly affects the output signal.

Practical value. The obtained results can be used to build systems for diagnosing interturn insulation of windings of electrical machines, in particular, as a methodological basis for diagnostic devices based on the use of the proposed approach.

Keywords: *impulse processes, insulation diagnostics, wet windings, simulation modeling*

Received: 26 January 2026
Accepted: 28 May 2026
Available online: 27 August 2026

Introduction. Electrical machines are widely used in various branches of industry and in everyday life, and it is difficult to imagine a modern enterprise or household that does not use at least one electrical machine in one form or another [1]. The issue of reliability of any technical devices, equipment, or systems is extremely important and cannot be resolved once and for all; it is only possible to continuously improve diagnostic methods and tools, develop fundamentally new diagnostic approaches, and so on [2].

This paper is devoted to diagnosing one of the most vulnerable components of the active part of electrical machines, namely their multi-turn random-wound winding.

Electrical machines, as the most widespread type of electromechanical energy converters, consume a significant amount of electrical energy overall and perform numerous important technological functions. Any improvement or refinement of them, even by fractions of a

© Kovalenko M. A., Chumack V. V., Tsyplenkov D. V., Dukhno R. P., Horbatko D. D., 2026

percent, has a substantial economic impact and effect. Global factors such as deglobalization, higher import taxes, and increased demand for metals used in electrical machines imply only a further increase in their cost, and in the future this increase may become quite rapid [3, 4]. Therefore, the relevance of repair, maintenance, and life extension of electrical machines performing important technological functions is also increasing. Fulfillment of these operational tasks requires modern, affordable, user-friendly, and reliable means for diagnosing the most vulnerable active parts of an electrical machine. In the manufacturing process, the issue of reliability has always been and remains one of the most important and relevant [5].

For this very reason, as one of the steps toward developing a device for the impulse diagnostics of the insulation condition of electrical machine windings during manufacturing, scheduled maintenance, and repair, there is a need for a well-founded approach both to the selection of the material of the sensor and the inductor and to the pulse parameters. This is because timely detection of defects, especially those at an early stage of development, can prevent sudden equipment failure and significant capital and material costs. All of the above confirms the relevance of the subject of this paper.

In papers [6, 7], the authors model the skin effect on the basis of the field diffusion equation, studying how the skin effect influences the field distribution across the sheet thickness and the associated losses. In [6], numerical methods are used to solve the field diffusion equation, and it is concluded that at a frequency of 50 Hz the influence of the skin effect can be neglected. In [7], an analytical method is used for the field diffusion equation, and analytical expressions are proposed for calculating the eddy-current loss component with the skin effect taken into account.

Papers [8, 9] focus more on the fundamental principles of the behavior of magnetic permeability and losses in ferromagnetic materials as the frequency changes. Paper [8] studies high-frequency losses when different electrical steels are used and at different values of magnetic induction. A loss model and a model of the influence of the skin effect on losses at high values of magnetic induction and frequency, that is, under the nonlinear influence of the skin effect, are developed in that work. Paper [9] shows that the effective magnetic permeability depends on the average value of the sinusoidal excitation voltage and does not change within one sinusoidal cycle even at high values of magnetic induction. Diffusion through metal is not wave-like at all, but rather represents simple exponential attenuation with an insignificant time delay and almost zero phase shift.

Studies [10, 11] focus on loss models in electrical steel as functions of magnetic induction and frequency and include different approaches to separating losses into components and accounting for eddy currents [12, 13], not through field diffusion but by means of analytically or experimentally fitted expressions. Paper [10] proposes a model for calculating losses in a magnetic core taking into account microscopic eddy currents, as well as a method for reproducing the shape of the dynamic hysteresis loop and losses under a sinusoidal excitation waveform up to high frequencies over a wide range of magnetic induction and excitation frequency. Paper [11] proposes a method for estimating losses in a laminated core subjected to high-frequency and nonsinusoidal excitation using only low-frequency measurements. The proposed model takes into account the nonuniform distribution of the magnetic field inside a laminated sheet and the hysteresis loop. Study [12] analyzes the effect of the skin effect on the application of Bertotti's formula to describe energy losses in electrical steel. The paper determines the maximum frequency at which the influence of the skin effect on the distribution of magnetic flux in electrical steel remains insignificant. In paper [13], an eddy-current power loss model is implemented, and it is shown that the magnetization frequency and the peak magnetic induction are the two determining factors that significantly affect the magnetic properties of electrical steels.

Papers [14, 15] investigate iron losses considering the electrical machine as a whole rather than only its core. Paper [14] presents a modeling approach for accounting for core losses in an electrical machine generated by higher harmonics of the supply voltage frequency. The model is based on a post-processing calculation tool for taking into account the magnetic skin effect in laminated electrical-steel sheets at high frequencies. Study [15] presents a method for calculating core losses in rotating electrical machines considering the skin effect and excess losses in the stator and rotor. The analysis takes into account eddy currents along the axial direction inside an electrical-steel sheet and considers the influence of the molecular structure of the steel by means of an experimental eddy-current loss modification coefficient.

As a result of the conducted literature search and analysis, it can be concluded that modern scientific research in the field of high-frequency impulse processes is aimed at studying the mechanisms of interaction between the electromagnetic field and eddy currents, the dependence of magnetic permeability on the supply frequency, and the nature of losses in electrical steels. Thus, the main research studies are focused on finding effective approaches to describing high-frequency losses and field diffusion processes [16], which are important in the design and diagnostics of modern electromechanical systems [17].

Therefore, the relevance of this study is determined by the need to improve the accuracy, speed, and reliability of non-destructive methods for assessing the condition of the inter-turn insulation of random-wound windings in electrical machines. The proposed method is based on impulse processes in which electromagnetic phenomena are determined not by stationary but by transient characteristics of the material. The use of different materials for the sensor and the inductor of the diagnostic system results in fundamentally different impulse response mechanisms, different rates of diffusion and attenuation of the electromagnetic field, which affects losses, heating, amplitude-frequency characteristics, and the sensitivity of measuring systems [18]. In this regard, it is relevant to compare impulse processes in ring cores made of different materials, which will make it possible to determine their suitability for use under fast transient conditions, optimize the design of components of diagnostic devices, and improve the efficiency of impulse electromagnetic diagnostic systems.

The purpose of this study is to develop a three-dimensional numerical circuit-field mathematical model of impulse processes in magnetic cores made of ferrite and thin-sheet electrical steel in order to assess impulse overvoltages in the diagnosis of inter-turn short circuits in electrical machine windings.

Results. The computational domain used to study impulse processes in the studied system is shown in Fig. 1.

The inductor winding and the sensor winding are made of copper winding wire and have a sufficient number of turns to provide the required magnitude of the studied voltage impulse (>100 V per turn).

The magnetic cores of the inductor and the sensor are made of electrical materials with different properties: ferrite material, thin-sheet electrical steel, or conventional electrical steel with a thickness of 0.5 mm.

The studied multi-turn winding is modeled as a solid piece, which is artificially divided into elementary conductors. The simulation of the number of inter-turn short circuits and their severity is carried out by changing the conductivity of the studied winding array or the current magnitude in it.

The auxiliary magnetic core performs the function of a magnetic flux concentrator and makes it possible to approximate the diagnostic process on the studied prototype as closely as possible to real conditions. For this reason, the magnetic core is made of 0.5 mm electrical steel, and the design of the auxiliary magnetic circuit makes it possible to vary the distance between the magnetic core of the inductor and that of the sensor. The distance between these cores also affects the error in the excitation of impulse transient processes in the studied system.

The main parameters and characteristics of the individual elements of the studied numerical simulation model are given in Table 1.

The data in Table 1 is used to develop the geometry of the computational domain, followed by the import and configuration of the parameters of all computational elements of the computational domain in the COMSOL Multiphysics environment implementing the finite element method. Depending on the stated computational task and the parameters of the magnetic cores of the inductor and the sensor, the material properties and the system of nonlinear differential equations are defined.

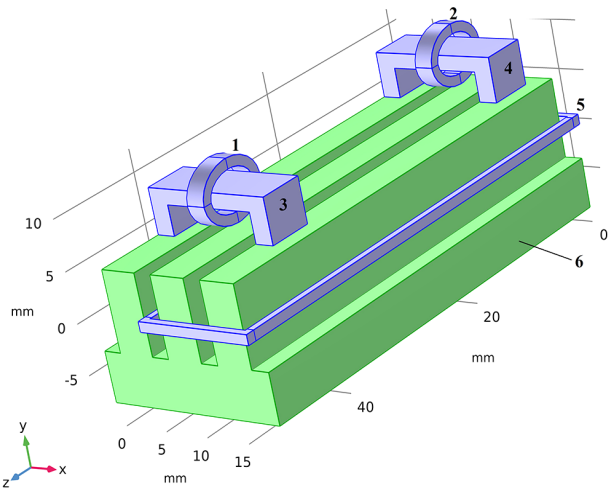

Fig. 1. Structure of the studied system for impulse processes:

1 – inductor winding; 2 – sensor winding; 3 – magnetic core of the inductor; 4 – magnetic core of the sensor; 5 – tested multi-turn winding; 6 – auxiliary magnetic core

The calculation result is obtained by the finite element method in a three-dimensional formulation under the following assumptions:

1. To simulate the laminated structure of the magnetic core when laminated electrical steel is used for the magnetic core of the sensor, the inductor, and the auxiliary core, anisotropic electrical conductivity properties are assigned to the corresponding computational domains.

2. The electrical conductivity of the electrical steel and the ferrite magnetic core is assumed to be homogeneous along each of the x, y, and z axes.

3. Changes in material properties with temperature are not taken into account, since under impulse operat-

Table 1

Main parameters and characteristics of the studied system

No.	Parameter	Value
1	Axial length of the auxiliary magnetic core, mm	50.0
2	Width of the auxiliary magnetic core, mm	20.0
3	Height of the auxiliary magnetic core, mm	13.00
4	Material of the auxiliary magnetic core	Steel 2411
5	Number of turns of the inductor/sensor winding	5/40
6	Excitation current in the inductor winding, A	75.0
7	Diameter of the winding wire of the inductor/sensor winding, mm^2	4.0/0.01
8	Width of the magnetic core of the inductor/sensor, mm	14.0
9	Axial length of the magnetic core of the inductor/sensor, mm	5.0
10	Magnetic permeability of the ferrite material of the inductor/sensor magnetic core, rel. units	≈2,000
11	Electrical conductivity of the ferrite material of the inductor/sensor magnetic core, S/m	$1 \cdot 10^{-3}$
12	Thickness of an individual lamination of the thin-sheet magnetic core material, mm	0.03
13	Magnetic permeability of the thin-sheet material of the inductor/sensor magnetic core, rel. units	1,250
14	Electrical conductivity of the thin-sheet material of the inductor/sensor magnetic core, S/m	$1.5 \cdot 10^6$
15	Magnetic permeability of the 2011 electrical steel of the inductor/sensor magnetic core, rel. units	700
16	Electrical conductivity of the 2011 electrical steel of the inductor/sensor magnetic core, S/m	$1.1 \cdot 10^7$
17	Number of turns of the test winding	25
18	Diameter of the winding wire of the test winding, mm	0.50

ing conditions the current magnitude is not high and does not lead to temperature variation over a wide range.

4. The windings are modeled as homogeneous conductive regions, since modeling each conductor separately would lead to an excessive increase in the number of unknowns and a significant increase in the model computation time.

The developed numerical simulation model of impulse processes in magnetic cores is characterized by the computational domain (Fig. 1) and the material properties of its individual structural components (Table 1), while the distribution of the electromagnetic field and eddy currents within it is described by the system of equations given below.

The system of coupled equations describing the distribution of the three-dimensional electromagnetic field in the studied system for the impulse diagnosis of interturn insulation is written in terms of the complex amplitude of the magnetic vector potential A [19]

$$\vec{A} = \vec{e}_x \cdot \dot{A}_x + \vec{e}_y \cdot \dot{A}_y + \vec{e}_z \cdot \dot{A}_z,$$

and the scalar electric potential φ is written in the form of the following system of equations [20]

$$\nabla \times \left(\frac{1}{\mu} \nabla + \vec{A} \right) + j\omega\sigma \cdot \vec{A} + \sigma \nabla \varphi = \vec{J}_e;$$

$$\nabla \cdot \left(j\omega\sigma \cdot \vec{A} + \sigma \nabla \varphi - \vec{J}_e \right) = 0,$$

where ω is the angular frequency of variation of the quantities with time; μ is the magnetic permeability; σ is the electrical conductivity of the material; J_e is the spatial current density vector, which is specified in the form of a pulse in the excitation winding and consists of three spatial components

$$\vec{J}_e = \vec{e}_x \cdot \dot{J}_{ex} + \vec{e}_y \cdot \dot{J}_{ey} + \vec{e}_z \cdot \dot{J}_{ez}.$$

The current in the inductor winding is specified as a pulse with such an amplitude and rise time that a pulse EMF with a maximum amplitude of >100 V is induced in the measuring winding. The current with a rise time Δt is specified by the approximation of a linear rise

$$i(t) = \begin{cases} 0, & t < t_0 \\ \dfrac{I_0}{\Delta t}\left(t - t_0\right), & t_0 \le t < t_0 + \Delta t, \\ I_0, & t \ge I_0 + \Delta t \end{cases} \qquad (1)$$

where Δt is the rise time of the current pulse, s; t_0 is the moment when the current pulse begins to rise, s; I_0 is the final (maximum) or steady-state value of the current step in the inductor winding, A.

The expression

$$\frac{I_0}{\Delta t}\left(t - t_0\right), \qquad (2)$$

within the system of equations (1) represents a linear function that defines a smooth increase in the current from 0 to the specified value I_0 over the time interval Δt. Expression (2) simulates a non-ideal current step that occurs in real impulse tests and takes into account the presence of inductance, eddy currents, and hysteresis phenomena in the magnetic cores.

Then, the effective value of the current density in the inductor winding is specified as follows

$$J_e = \frac{W \cdot i(t)}{S_i},$$

where W is the number of turns in the inductor winding; S_i is the equivalent area occupied by the inductor winding, mm^2.

The induced electromotive force is determined with respect to the magnetic vector potential A. For this purpose, the magnetic flux Φ, linked with the sensor winding (or measuring winding) is determined

$$\Phi = \sum A_e^n \cdot l_e, \qquad (3)$$

where A_e is the average value of the magnetic vector potential at an arbitrary moment t^n in individual e-elements of finite-element mesh; l_e is the contour length, or the mean length of the excitation winding.

After calculating the magnetic flux using expression (3), the magnitude and waveform of the EMF in the sensor winding are determined at each moment t^n

$$E = -W \cdot \frac{1}{\Delta t} \sum \left(A_e^n - A_e^{n-1} \right) \cdot l_e.$$

The calculation is performed taking into account the losses arising in the magnetic cores of the individual elements of the studied system: the auxiliary core and the magnetic cores of the inductor and the sensor. To take these losses into account, the following expression is used

$$Q_j = 1/T \int_{T_1 - T}^{T_1} J \cdot E dt,$$

where T, T_1 are the period of the current pulse arising in the inductor winding; J is the current density in the individual computational domains; E is the electric field strength vector.

To implement the studied numerical simulation model and obtain reliable results, the minimum number of finite elements in the mesh must be approximately 600 thousand. A fragment of the finite-element mesh of the studied model in the region of the inductor winding is shown in Fig. 2.

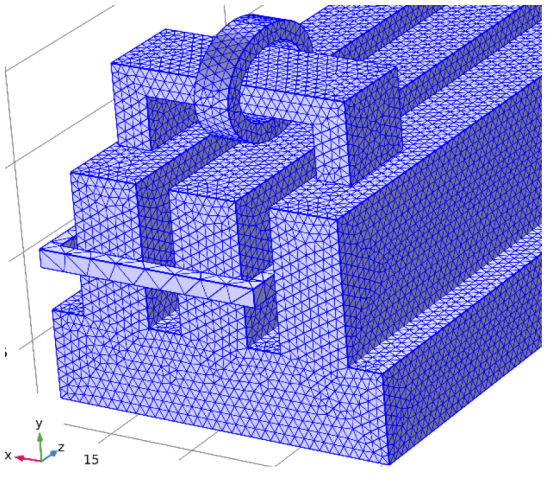

Fig. 2. Part of the finite-element mesh of the computational domain

The winding parameters were taken into account by homogenizing their multi-turn structure into a continuous electrically conductive body with equivalent electromagnetic properties, which makes it possible to preserve the computational convergence of the model when using the specified number of finite elements without the need to represent each individual turn in detail. The geometric parameters of the section are determined by the number of turns $W = 25$ (Table 1) and the winding-wire diameter $d = 0.5$ mm, which defines the outer dimensions of the winding and its location in the working gap between the auxiliary core, the inductor, and the sensor.

The simulation of the presence of inter-turn short circuits was implemented by changing the electrical conductivity of the winding material: from the nominal conductivity of copper (defect-free condition) to a conditionally infinite conductivity corresponding to the appearance of short-circuited turns (2, 3, or 4 short-circuited turns). This approach makes it possible to adequately reproduce the occurrence of additional eddy currents in the damaged winding section and their influence on the overall transient process in the system. The relationship between the winding section and the magnetic flux was taken into account by specifying boundary conditions on the winding surface with allowance for its actual location relative to the auxiliary magnetic core (item 6 in Fig. 1), with an axial length of 50 mm and the possibility of varying the distance between the inductor and sensor cores, which directly affects the electromagnetic coupling coefficient and the diagnostic sensitivity.

The result of the calculation of the electromagnetic field distribution in the studied system is shown in Fig. 3.

The electromagnetic field distribution (Fig. 3) is shown for the moment of time 5 μs, which corresponds to the decay of eddy currents in the magnetic cores of the inductor, the sensor, and the auxiliary core. Higher values of magnetic induction (background shading) correspond to the location of the winding and magnetic core of the inductor.

To provide the excitation required for diagnostics in terms of the magnitude of the electromagnetic field and the currents in the sensor winding, the current pulse in the primary winding must ensure an EMF in the sensor winding with a maximum amplitude of up to 100 V. When the inductor winding is switched by a direct current with an amplitude of approximately 90 A and a pulse rise time of 1 μs, a transient process with a free decaying

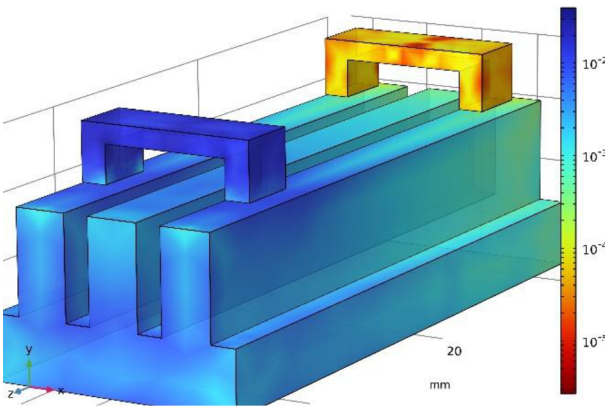

Fig. 3. Electromagnetic field distribution in the inductor-sensor system

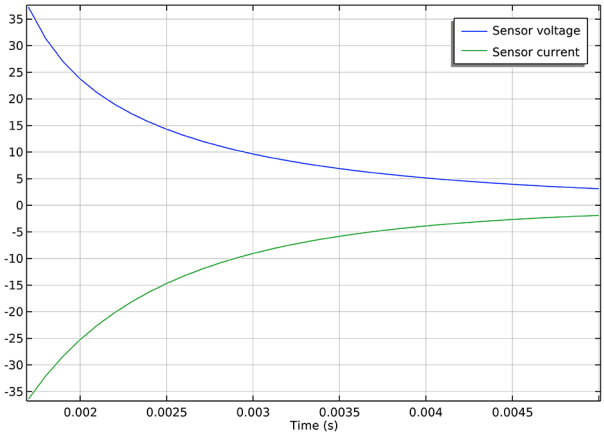

Fig. 4. Time dependence of the EMF and current in the sensor winding

component arises in the studied system. In this case, the current and EMF in the sensor winding are aperiodic in nature and have the form shown in Fig. 4.

The dependences in Fig. 4 were obtained using inductor/sensor cores made of 2011 electrical steel, 0.5 mm thick.

To ensure an unambiguous physical interpretation of the obtained results, the developed three-dimensional numerical model introduces a consistent definition of the positive directions of the variables and takes into account the design parameters of the test winding section.

The system of equations (1–3) is solved in the Cartesian coordinate system (x, y, z), where the positive direction of the z-axis is oriented from the magnetic core of the inductor to the core of the sensor along the axis of symmetry of the system (Fig. 1). For the vector quantities, the following positive-direction conventions are adopted: the magnetic vector potential A has a positive direction coinciding with the direction of the magnetic flux density B in the air gap between the cores; the excitation current density J_e is defined as positive when the current in the inductor winding creates a magnetic flux directed along the z-axis from the inductor to the sensor. The EMF E in the sensor winding is determined according to the law of electromagnetic induction $d\Phi/dt$, which ensures the physical adequacy of the obtained dependences, in particular the phase opposition of the current and EMF in the measuring winding (Fig. 4).

The nature of the variation of the EMF and current in the sensor winding corresponds to the physical processes of electromagnetic wave penetration into an electrically conductive and magnetically permeable medium. At the same time, the two quantities are in phase opposition: the EMF has a sign opposite to that of the current, which is consistent with the law of electromagnetic induction. In Fig. 4, the maximum current amplitude is approximately 0.035 A, the voltage amplitude is approximately –35 V, and the decay time of the transient process is $\tau \approx 3.67$ μs. The amplitude and decay time of the transient aperiodic process may be regarded as diagnostic features indicative of the degree of defect development (Fig. 5).

Fig. 5 shows that when an inter-turn short circuit appears in the test winding, the signal amplitude decreases, while the duration of the transient process increases. This can be explained by the fact that the currents in the

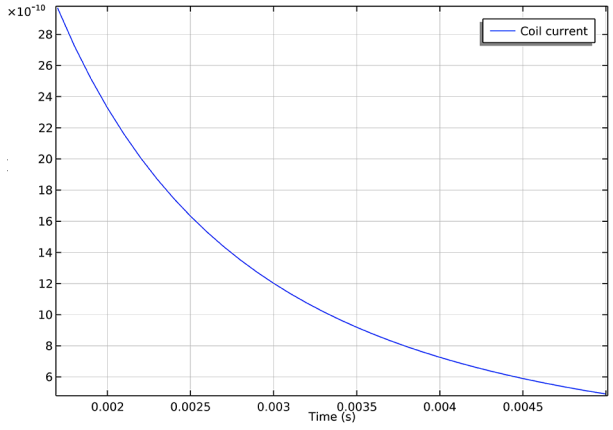

a

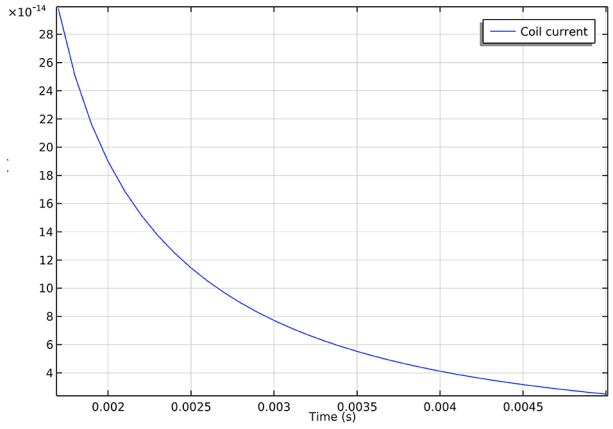

b

Fig. 5. Current in the sensor winding for:

a – the presence of an inter-turn short circuit in the test winding; b – a defect-free winding

short-circuited turn contribute to an increase in the magnetic flux decay time in the system and, consequently, in the decay time of the EMF and currents in the sensor winding.

A comparison of the dependences obtained in Fig. 5 shows that the presence of an inter-turn short circuit is accompanied by a sharp increase in the current in the damaged winding section by 3 to 4 orders of magnitude. This makes it possible to use the magnitude of the induced current as a sensitive diagnostic feature. At the same time, the current amplitude and decay rate correlate with the number of short-circuited turns and the degree of damage, which makes it possible not only to detect the defect but also to quantitatively assess the degree of its development.

To assess the influence of the type of magnetic core material of the inductor and the sensor on the detection of inter-turn insulation damage in the test winding, a series of calculations was carried out. In doing so, the degree of defectiveness of the test winding was varied: 2, 3, and 4 short-circuited turns.

The results of calculating the amplitude of EMF and the decay time τ of the transient process for different types of magnetic cores and different degrees of defectiveness of the test winding are presented in Table 2.

In Table 2, the number of short-circuited turns equal to "1" means that the winding is defect-free, that is, no short-circuited turns are present.

Table 2

Calculated amplitude and decay time of the transient process

SC turns	Ferrite core		Thin-sheet core		2011 steel core	
	Amplitude, V	decay time, μs	Amplitude, V	decay time, μs	Amplitude, V	decay time, μs
1	248	61	173	47	92	31
2	204	67	157	54	87	38
3	147	79	124	63	79	46
4	103	87	91	68	67	51

When ferrite cores are used for the sensor and the inductor, the highest pulse amplitude values (248–103 V) are observed compared with the use of cores made of thin-sheet electrical steel (173–91 V) or 2011 steel (31–51 V) for any number of short-circuited turns. This is explained by the low electrical conductivity of the ferrite material, which results in a minimal magnitude of eddy currents in the magnetic cores of the sensor and the inductor; therefore, a significant portion of the pulse energy is converted into the magnetic field and induces a high-amplitude EMF pulse in the sensor winding. At the same time, the high magnetic permeability of the ferrite core promotes substantial storage of magnetic energy, which contributes both to a slower decay of the transient process and to an increase in the amplitude of the induced EMF in the sensor winding. In addition, the longest decay time of the transient process (61–131 μs) is observed when ferrite cores are used for the sensor and the inductor. This is due to the fact that ferrite cores are characterized by the lowest eddy-current losses; accordingly, the pulse energy dissipates slowly, and as a result the transient process lasts the longest in comparison with other types of magnetic cores.

The use of thin-sheet steel provides intermediate values of the pulse amplitude in the measuring winding, since its electrical conductivity is higher than that of the ferrite core and lower than that of 2011 steel. The presence of interlaminar insulation reduces eddy-current losses, which decreases their influence and shortens the decay time (37–124 μs) of the transient process.

The lowest signal amplitude in the sensor winding (≈ 92 V) is observed when the sensor and inductor cores are made of 2011 electrical steel with a thickness of 0.5 mm. This is explained by the action of relatively large eddy currents, which produce the strongest opposition to the main magnetic flux of the impulse excitation, since this steel grade has the highest electrical conductivity.

The dependence of the relative change in the signal amplitude of the sensor winding ΔA, %, on the number of short-circuited turns n in the test winding is shown in Fig. 6.

To analyze the variation in the signal amplitude as a function of the number of short-circuited turns, an exponential dependence of the following form is used

$$A(n) = A_0 \cdot e^{-\alpha n}, \qquad (4)$$

where A_0 is the signal amplitude for the defect-free test winding ($n = 0$); α is the signal damping (attenuation) coefficient corresponding to the appearance of (n) short-circuited turns.

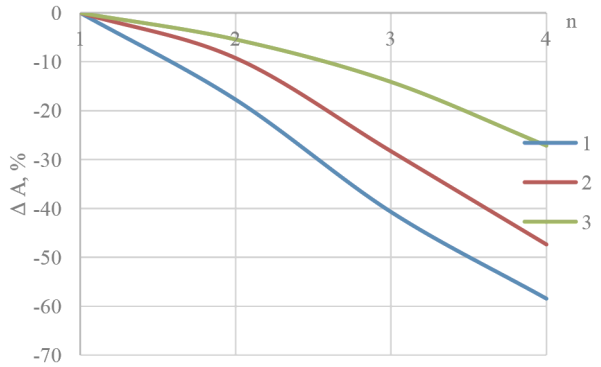

Fig. 6. Variation in the sensor winding amplitude as a function of the number of short-circuited turns:

curve 1 – variation in the signal amplitude of the sensor winding when ferrite cores are used for the sensor and the inductor; curve 2 – variation in the signal amplitude of the sensor winding when thin-sheet steel cores are used for the sensor and the inductor; curve 3 – variation in the signal amplitude of the sensor winding when 2011 steel is used as the core material for the sensor and the inductor

As a result, using expression (4), the following values of the coefficient α were obtained for the occurrence of short-circuited turns in the test winding ($n = 2, 3, 4$):

- for ferrite cores of the sensor and the inductor: $\alpha_f \approx 0.29$ (for $A_1 = 248$, $A_4 = 103$);
- for thin-sheet steel cores of the sensor and the inductor: $\alpha_{th} \approx 0.22$ (for $A_1 = 173$, $A_4 = 91$);
- for 2011 steel cores of the sensor and the inductor: $\alpha_s \approx 0.11$ (for $A_1 = 92$, $A_4 = 67$).

Thus, the greater the damping coefficient α, the higher the sensitivity of the output signal to the appearance of defects in the form of short-circuited turns. The use of ferrite shows the highest sensitivity of the sensor winding signal amplitude A to the appearance of defects in the test winding, both relative to the initial signal level A_0 and relative to the other two types of magnetic cores

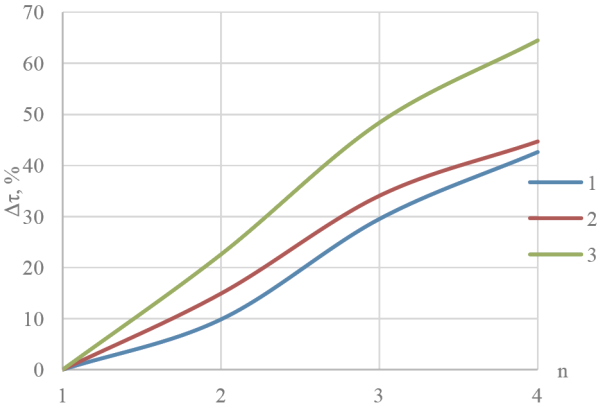

Fig. 7. Variation in the decay time as a function of the number of short-circuited turns:

curve 1 – relative variation in the signal decay time of the sensor winding when ferrite cores are used for the sensor and the inductor; curve 2 – relative variation in the signal decay time of the sensor winding when thin-sheet steel cores are used for the sensor and the inductor; curve 3 – relative variation in the signal decay time of the sensor winding when 2011 steel is used as the magnetic core material for the sensor and the inductor

used for the sensor and the inductor. This is clearly seen from the calculation results shown in Fig. 6.

Fig. 7 shows the dependence of the decay time of the transient process in the sensor winding on the number of short-circuited turns in the test winding.

The decay time of the transient process can be expressed by a linear dependence as a function of the number of short-circuited turns

$$\tau(n) = \tau_0 + \beta(n - 1),$$

where τ_0 is the duration of the transient process in the absence of short-circuited turns in the test winding; β is the average increment of the decay time of the transient process with an increase in the number of short-circuited turns n. As a result, we obtain:

- for ferrite cores of the sensor and the inductor: $\tau_0 = 61$ μs, $\beta_f = 23$ μs/turn;
- for thin-sheet steel cores of the sensor and the inductor: $\tau_0 = 47$ μs, $\beta_{th} = 33$ μs/turn;
- for 2011 steel cores of the sensor and the inductor: $\tau_0 = 31$ μs, $\beta_s = 6.7$ μs/turn.

Despite the fact that the smallest average increment in the decay time of the transient process, β_s, is observed when magnetic cores of 2011 steel are used for the sensor and the inductor, this material is characterized by the largest relative variation Δτ, % of the useful output signal (curve 3, Fig. 7). This feature can be used in the development of appropriate diagnostic equipment capable of detecting inter-turn short circuits in random-wound multi-turn windings with high accuracy and reliability.

The obtained values of the transient-process amplitude and decay time for different numbers of short-circuited turns have a clear physical interpretation. The character of the variation in the transient-process duration depends on the ratio between the effective inductance L_{eff} of the inductor–auxiliary core–test winding–sensor system and the effective resistance R_{eff}, as well as on the losses in the magnetic core and in the windings of the sensor and the inductor. An increase in the number of short-circuited turns simultaneously affects both the inductance and the equivalent resistance through the appearance of additional eddy currents in the system. For ferrite sensor and inductor cores, a change in the ratio L_{eff}/R_{eff} leads to a noticeable increase in the decay time of the transient process. For materials with high electrical conductivity (2011 steel), the increase in losses raises the value of the equivalent resistance R_{eff}, which leads to faster decay (damping) of the transient process.

Conclusions. A numerical circuit-field mathematical model of impulse processes in spatially displaced ring cores using different types of steel was developed in this study in order to assess the impulse overvoltages and decay times arising in the sensor winding. The obtained results showed that the type of magnetic core material of the sensor and the inductor has a significant effect on the parameters of the transient process and the amplitude of the induced EMF.

When ferrite cores are used, the highest EMF amplitudes in the sensor winding are observed (up to 248 V), as well as the longest decay time, up to 131 μs. When 2011 electrical steel is used for the cores, a maximum amplitude of 92 V is obtained with a minimum decay time of 31 μs, which is 50–80 % faster than for ferrite material. This confirms the feasibility of using ferrite

material for diagnostic tasks requiring increased sensitivity, while thin-sheet steel and 2011 steel are more suitable for fast impulse diagnostics.

A comparison of the transient-process decay rate showed that there is a clear tendency for τ to increase as the electrical conductivity of the material decreases. For the ferrite material of the sensor and inductor cores, which has the lowest electrical conductivity, the maximum decay time reaches 131 μs, whereas for 2011 steel it is 31 μs, that is, approximately 4.2 times faster. This is fully consistent with the physics of the processes within the system: at lower electrical conductivity of the material, the magnitude of the eddy currents is smaller, and accordingly the opposing action of these currents on the main impulse excitation flux is weaker, so the decay time increases.

When short-circuited turns appear in the test winding, the signal amplitude in the sensor winding decreases on average by 25–35 %, while the decay time increases by 40–60 %. This confirms the effectiveness of the impulse method for detecting short circuits in random-wound windings.

The results of the conducted study make it possible to formulate practical recommendations for selecting the materials of the magnetic cores of the sensor and the inductor for the development of highly sensitive sensors for monitoring inter-turn short circuits in random-wound windings of electrical machines. The developed model can serve as a basis for further optimization of the design of inductors and sensors for impulse diagnostics, as well as for the creation of hardware tools for the non-destructive testing of active materials of electrical machines.

Based on the obtained results, it is possible to develop diagnostic features and an appropriate methodology for devices intended for diagnosing inter-turn short circuits using impulse processes. The use of the method itself is promising for implementation in diagnostic systems for this type of damage.

References.

1. Kumar, L., Nadarajan, S., Vaiyapuri, V., Gupta, A. K., Soong, B. H., & Nguyen, H. D. (2020). Life estimation of electrical machine using aging model. *IECON 2020 – 46th Annual Conference of the IEEE Industrial Electronics Society*, 1034-1039. https://doi.org/10.1109/IECON43393.2020.9254606

2. Eckert, M., Mraz, P., Ballweg, C., & Pihera, J. (2025). Partial discharge behavior and insulation failures detection in electrical devices subjected to impulse voltage excitation. *International Journal of Electrical Power & Energy Systems*, 111078. https://doi.org/10.1016/j.ijepes.2025.111078

3. European Central Bank (2024). *Navigating a fragmenting global trading system: Insights for central banks* (Occasional Paper Series No. 365). https://doi.org/10.2866/9822653

4. International Energy Agency (2025). *Critical minerals*. https://www.iea.org/topics/critical-minerals

5. Psarommatis, F., May, G., Dreyfus, P. A., & Kiritsis, D. (2019). Zero defect manufacturing: State-of-the-art review, shortcomings and future directions in research. *International Journal of Production Research, 58*(1), 1-17. https://doi.org/10.1080/00207543.2019.1605228

6. Decner, A., Baranski, M., Jarek, T., & Berhausen, S. (2022). Methods of Diagnosing the Insulation of Electric Machines Windings. *Energies, 15*(22), 8465. https://doi.org/10.3390/en15228465

7. Li, J., Yang, Q., Wang, S., & Li, Y. (2018). Skin effect and eddy current loss in electrical steel sheets under applied excitation fields. *2018 IEEE International Magnetics Conference (INTERMAG)*, 1. https://doi.org/10.1109/INTMAG.2018.8508090

8. Hofman, A., Bird, J. Z., & Kadel, K. (2023). A Multi-Stage Magnetic Gear. *IEEE Transactions on Magnetics, 59*(11), 1-5. https://doi.org/10.1109/TMAG.2023.3284421

9. Payne, A. (2024). *Skin effect in ferromagnetic materials (Issue 2) and the averaging of magnetic permeability*. https://www.researchgate.net/publication/377703071_SKIN_EFFECT_IN_FERROMAGNETIC_MATERIALS_ISSUE_2_AND_THE_AVERAGING_OF_MAGNETIC_PERMEABILITY

10. Petrun, M., & Steentjes, S. (2020). Iron-loss and magnetization dynamics in non-oriented electrical steel: 1-D excitations up to high frequencies. *IEEE Access, 8*, 4568-4593. https://doi.org/10.1109/ACCESS.2019.2963482

11. Ibrahim, M., & Pillay, P. (2012). Core loss prediction in electrical machine laminations considering skin effect and minor hysteresis loops. *2012 IEEE Energy Conversion Congress and Exposition (ECCE)*, 2681-2687. https://doi.org/10.1109/ECCE.2012.6342536

12. Bereźnicki, M. (2015). The influence of skin effect on the accuracy of eddy current energy loss calculation in electrical steel sheets. *2015 Selected Problems of Electrical Engineering and Electronics (WZEE)*, 1-4. https://doi.org/10.1109/WZEE.2015.7394046

13. Hamzehbahmani, H., Anderson, P., & Preece, S. (2015). Application of an advanced eddy-current loss modelling to magnetic properties of electrical steel laminations in a wide range of measurements. *IET Science, Measurement & Technology, 9*, 807-816. https://doi.org/10.1049/iet-smt.2014.0276

14. Rens, J., Vandenbossche, L., & Dorez, O. (2020). Iron loss modelling of electrical traction motors for improved prediction of higher harmonic losses. *World Electric Vehicle Journal, 11*(1), 24. https://doi.org/10.3390/wevj11010024

15. Sirizzotti, B., Addae, D., Agamloh, E., von Jouanne, A., & Yokochi, A. (2025). A Review of Stator Insulation State-of-Health Monitoring Methods. *Energies, 18*(14), 3758. https://doi.org/10.3390/en18143758

16. Chumak, V. V., Kovalenko, M. A., Trotsenko, Y. O., Stulishenko, A. S., & Tymoshchuk, O. L. (2022). High-frequency methods for detecting insulation defects in mesh winding generators of power plants based on renewable energy sources. *Vidnovluvana Energetika*, *4*(71), 56-63. https://doi.org/10.36296/1819-8058.2022.4(71).56-63

17. Chumack, V., Kovalenko, M., Tymoshchuk, O., Stulishenko, A., & Ihnatiuk, Y. (2023). Design of a multilink system for calculating high-frequency processes in electric machines with mesh windings. *Eastern-European Journal of Enterprise Technologies, 3*(8(123)), 54-63. https://doi.org/10.15587/1729-4061.2023.282375

18. Chumack, V., Tymoshchuk, O., Kovalenko, M., Bazenov, V., Ihnatiuk, Y., & Stulishenko, A. (2023). Research of high-frequency remagnetization model in laminated magnetic cores of electromechanical and electromagnetic energy converters. *Eastern-European Journal of Enterprise Technologies, 4*(5(124)), 6-15. https://doi.org/10.15587/1729-4061.2023.286002

19. Wang, J., Kong, Y., Cai, Y., & Wang, Y. (2024). Effect of the repetition frequency and polarity of square wave voltage on the partial discharge of electric machine insulation for more electrical aircraft. *Journal of Physics: Conference Series*, *2820*(1), 012110. https://doi.org/10.1088/1742-6596/2820/1/012110

20. Chumack, V., Kovalenko, M., Tymoshchuk, O., & Dukhno, R. (2025). Detecting insulation defects in electrical machines' multi-turn windings based on analysis of transient electromagnetic processes. *Eastern-European Journal of Enterprise Technologies, 5*(5(137)), 19-30. https://doi.org/10.15587/1729-4061.2025.342301

Порівняння імпульсних процесів у просторово зміщених кільцеподібних осердях із фериту й тонколистової сталі

М. А. Коваленко[1], *В. В. Чумак*[1], *Д. В. Ципленков*[*2,3], *Р. П. Духно*[1], *Д. Д. Горбатко*[1]

1 – Національний технічний університет України «Київський політехнічний інститут імені Ігоря Сікорського», м. Київ, Україна

2 – Національний технічний університет "Дніпровська політехніка", м. Дніпро, Україна

3 – Дніпропетровський науково-дослідний інститут судових експертиз, м. Дніпро, Україна

* Автор-кореспондент e-mail: tsyplenkov.d.v@nmu.one

Мета. Розробка чисельної імітаційної моделі імпульсних процесів магнітних осердь із фериту

й тонколистової електротехнічної сталі з метою оцінки величини імпульсних перенапруг.

Методика. Розподіл електромагнітного поля й вихрових струмів розраховувався із використанням методу скінченних елементів. Засоби автоматизованого проєктування використовувалися для розробки геометричних моделей розрахункової області досліджуваних процесів у кільцеподібних осердях. Для збудження імпульсних процесів у досліджуваній системі використовувалась теорія перехідних процесів і закони електричних кіл.

Результати. Розроблена тривимірна чисельна коло-польова математична модель імпульсного збудження кільцеподібних осердь із різних матеріалів електротехнічної сталі давача й індуктора, що використовується для діагностування міжвиткових замикань всипних обмоток. Модель дозволяє визначати часові залежності струму, напруги й характер зміни магнітного потоку при проходженні імпульсного фронту збудження. Отримані розподіли електромагнітного поля, вихрових струмів і динаміку їхнього затухання для різних значень магнітної проникності й електропровідності матеріалів. Отримані результати дозволяють кількісно оцінити вплив параметрів матеріалів на імпульсні процеси, визначити межі ефективності застосування феритових осердь з різних типів електротехнічної сталі у високочастотних системах діагностування, сенсорах і перетворювачах енергії.

Наукова новизна. Результати аналізу чисельного імітаційного моделювання досліджуваної системи показали, що в залежності від типу матеріалу осердя процеси хвильового проникнення з мінімальними втратами притаманні для феритового матеріалу. У тонколистовій сталі вихрові струми в кожному окремому листі здійснюють значний вплив на екранування імпульсу, що суттєво впливає на вихідний сигнал.

Практична значимість. Отримані результати можливо використовувати для побудови систем діагностування міжвиткової ізоляції обмоток електричних машин, зокрема, як методологічну основу для пристроїв діагностування, що базуються на використанні запропонованого підходу.

Ключові слова: *імпульсні процеси, діагностування ізоляції, всипні обмотки, імітаційне моделювання*